Cancer Letters 454 (2019) 53–65

Contents lists available at ScienceDirect

Cancer Letters

journal homepage: www.elsevier.com/locate/canlet

Original Articles

Pseudophosphatase STYX promotes tumor growth and metastasis by inhibiting FBXW7 function in colorectal cancer

Diao He[a,b,1], Zida Ma[a,b,1], Chao Fang[a,b,1], Jingjing Ding[a,1], Wenming Yang[a], Peng Chen[a], Libin Huang[a,b], Cun Wang[a], Yongyang Yu[a], Lie Yang[a,b,*], Yuan Li[b], Zongguang Zhou[a,b,**]

[a] Department of Gastrointestinal Surgery, West China Hospital, Sichuan University, Chengdu, 610041, Sichuan, China
[b] Institute of Digestive Surgery, State Key Laboratory of Biotherapy and Cancer Center, West China Hospital, Sichuan University, Chengdu, 610041, Sichuan, China

ARTICLE INFO

Keywords:
Protein tyrosine phosphatases
EMT
Oncogene
Prognostic biomarker

ABSTRACT

Serine/threonine/tyrosine interacting protein (STYX), a member of protein tyrosine phosphatases, has recently been reported as a potential oncogene. However, the role of STYX in colorectal cancer (CRC) remains unknown. In this study, we found that STYX was highly expressed in CRC tissues and closely correlated with tumor development and survival of CRC patients. *In vitro* studies showed that overexpression of STYX promoted proliferation, migration, invasion, and epithelial-mesenchymal transition (EMT) and inhibited apoptosis in CRC cells, while STYX knockdown had the opposite effects. Consistently, *in vivo* experiments showed that overexpression of STYX promoted tumor growth and lung metastasis. Mechanically, STYX bound to the F-box and WD repeat domain-containing7 (FBXW7) protein and inhibited its function. Co-regulation of STYX and FBXW7 expression reversed the biological changes mediated by regulation of STYX expression alone in CRC cells. Additionally, FBXW7 expression was negatively associated with STYX expression in CRC tissues, and low STYX levels accompanying high FBXW7 levels predicted favorable prognosis of CRC patients. In conclusion, our results suggest that STYX plays an oncogenic role by inhibiting FBXW7 and represents a potential therapeutic target and prognostic biomarker in CRC.

1. Introduction

As one of the most common malignant tumors, colorectal cancer (CRC) is the second leading cause of cancer-related deaths, with an estimated annual incidence of 1.4 million cases worldwide [1,2]. Despite recent curative improvements made in CRC therapy, the prognosis of CRC patients remains poor due to the lack of effective therapeutic targets [3,4]. Diverse signaling pathways and abnormally expressed genes involved in CRC have been identified, but the precise molecular mechanism of CRC is not fully understood. Thus, to improve the prognosis of patients with CRC, it is imperative to explore novel molecular markers that can better risk assessment and therapy.

Serine/threonine/tyrosine interacting protein (STYX), a prototypical pseudophosphatase, belongs to the family of protein tyrosine phosphatases (PTPs) [5]. STYX displays the structural features of PTPs but lacks an active catalytic loop. Within its phosphatase domain, the catalytic cysteine at position 120 is replaced by glycine, resulting in the lack of dephosphorylation function [6]. Although STYX is widely expressed in various tissues [6,7], less is known about its biological function as available studies are very limited. Wishart et al. [8] found that STYX combined with a testicular RNA binding protein, suggesting the potential role of STYX in spermatogenesis. Reiterer et al. [9] showed that STYX worked as a nuclear anchor for extracellular signal-regulated kinases 1/2 to modulate their nucleo-cytoplasmic shuttling.

A recent study implicated STYX as a potential oncogene, showing that STYX inhibited the apoptosis of breast cancer cells by binding the F-box and WD repeat domain-containing7 (FBXW7) protein with its expression negatively related to prognosis in breast cancer patients [10]. FBXW7 is a member of the F-box family that ubiquitinates substrate proteins in a variety of biological process [11–13] and has a high mutation frequency (9%) in colon cancer [14,15]. Strong evidence has demonstrated that FBXW7 plays a negative role in the pathogenesis of

Abbreviations: Serine/threonine/tyrosine interacting protein, (STYX); Colorectal cancer, (CRC); F-box and WD repeat domain-containing7, (FBXW7); short hairpin RNA, (shRNA); Cell Counting Kit-8, (CCK-8)

* Corresponding author. Department of Gastrointestinal Surgery, West China Hospital, Sichuan University, No. 37 Guoxue Lane, Chengdu, 610041, China.
** Corresponding author. Department of Gastrointestinal Surgery, West China Hospital, Sichuan University, No. 37 Guoxue Lane, Chengdu, 610041, China.
E-mail addresses: lie_222@163.com (L. Yang), zhou767@163.com (Z. Zhou).
[1] These authors contribute equally to the work.

https://doi.org/10.1016/j.canlet.2019.04.014
Received 22 December 2018; Received in revised form 14 March 2019; Accepted 9 April 2019

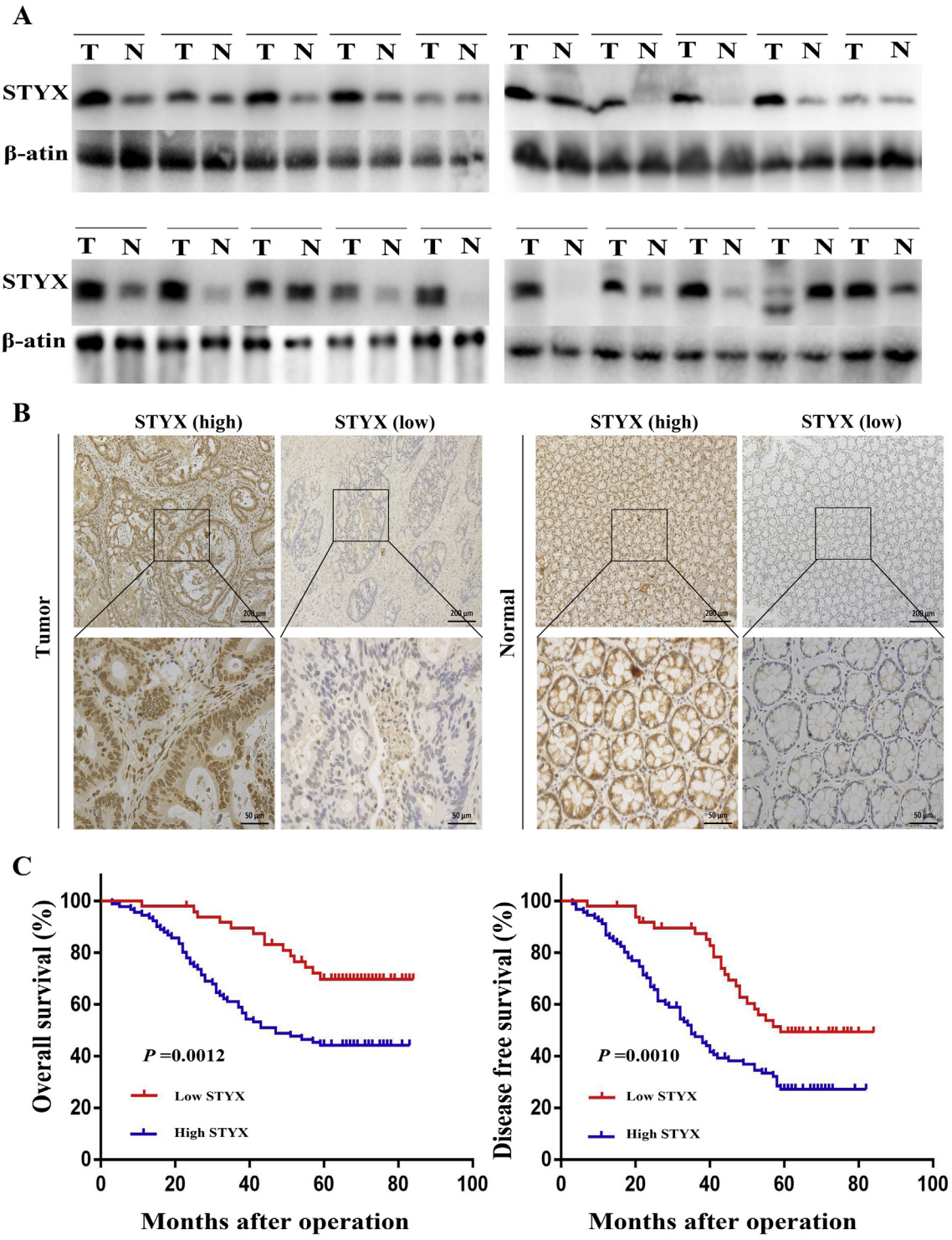

Fig. 1. STYX was up-regulated in CRC tissues. (A) STYX expression in 20 paired CRC samples as detected by Western blot analysis. (B) Immunohistochemical staining of STYX in tumor tissues and the matched normal tissues. (C) Kaplan–Meier survival analysis of overall survival and disease free survival according to the STYX expression in 140 CRC patients.

CRC [16–18], including inhibition of the proliferation and migration as well as the promotion of apoptosis of CRC cells [19–21]. The high expression of FBXW7 independently related to a favorable prognosis for CRC patients [22]. Based on this background, we propose a hypothesis that STYX may be involved in the pathogenesis of CRC by regulating FBXW7.

In this present study, STYX expression was examined both in CRC tumor tissues and normal tissues, the correlation between STYX expression and prognosis were studied, the direct role of STYX was assessed in the growth and metastasis of CRC, and the underlying molecular mechanism was investigated.

Table 1
Relation between STYX expression level and clinicopathologic features in 140 CRC patients.

Variables	Case (n = 140)	STYX expression		*P* value
		High (n = 91)	Low (n = 49)	
Age				0.282
< 65	59	35 (59.3%)	24 (40.7%)	
≥ 65	81	56 (69.1%)	25 (30.9%)	
Gender				0.379
male	64	39 (60.9%)	25 (39.1%)	
female	76	52 (68.4%)	24 (31.6%)	
Location[a]				0.302
Left sides	106	66 (66.2%)	40 (37.8%)	
Right sides	34	25 (73.5%)	9 (26.5%)	
Size (cm)				0.046*
< 5	55	30 (54.5%)	25 (45.5%)	
≥ 5	85	61 (71.8%)	24 (28.2%)	
Invasive depth				0.034*
T1 + T2	31	15 (48.4%)	16 (41.6%)	
T3 + T4	109	76 (69.7%)	33 (30.3%)	
Lymph node metastasis				0.017*
Absent	52	27 (51.9%)	25 (48.1%)	
Present	88	64 (72.7%)	24 (27.3%)	
Distant metastasis				0.543
M0	127	81 (63.8%)	46 (36.2%)	
M1	13	10 (76.9%)	3 (23.1%)	
TNM stages				0.009*
I + II	48	24 (50%)	24 (50%)	
III + IV	92	67 (72.8%)	25 (27.2%)	

[a]: Left sided: splenic flexure, descending colon, sigmoid colon, and rectum; Right sided: cecum, ascending colon, hepatic flexure, and transverse colon.
* Statistically significant.

2. Materials and methods

2.1. Cell culture and transfection

Human CRC cell lines (SW480, SW620, HCT116, HT29, RKO, and Lovo) were purchased from Procell Life Sciences Co. Ltd., (Wuhan, Hubei, China), and were recently authenticated by Procell Life Sciences Co. Ltd., using STR analysis [Supplementary materials]. The cell lines SW480, SW620, HCT116 and HT29 were cultured in DMEM supplemented with 10% fetal bovine serum (FBS). The Lovo cell line was maintained in Ham's F−12K medium with 10% FBS, and the RKO cell line was cultured in MEM with 15% FBS. All of these cells were incubated at 37 °C in an atmosphere of 95% air-5% CO_2.

The STYX-shRNA (LV-STYX-shRNA-Puromycin), STYX (LV-Flag-STYX-Puromycin), FBXW7-shRNA (LV-FBXW7-shRNA-Puromycin), FBXW7 (LV-Flag-FBXW7-Puromycin) and the negative control viruses were purchased from Genechem Co. Ltd. (Shanghai, China). The shRNA sequences used for targeting were as follows: STYX (#1) 5′-CCAGATA GAAAGGTCATTA-3′; STYX (#2) 5′-CTATGACTAAGGAATTTAT-3′; STYX (#3) 5′- CATATTCATCTGCTATGAA-3′; FBXW7 5′- AGAGAAATT GCTTGCTTTA-3′. The lentiviruses were transfected into CRC cells in presence of polybrene and selected in medium containing 2 μg/mL puromycin.

2.2. Tissue samples and immunohistochemistry (IHC)

A total of 140 CRC tissues and paired adjacent normal tissues were obtained from the West China Hospital (Chengdu, Sichuan, China) between 2009 and 2011. Written informed consent was obtained from the patients for publication of this manuscript, and the study was approved by the Biomedical Ethics Committee of West China Hospital. Immunohistochemistry was performed as previously described [23]. Briefly, after a series of previous steps, slides were incubated with primary antibodies including STYX (1:100, Abcam), FBXW7 (1:500, Abcam), and Ki-67 (1:500, Abcam), followed by incubation with HRP labeled secondary antibody.

Under high-power magnification (× 100), photographs of three representative fields were captured by the ZEN 2012 software (blue edition). Identical settings were used for each photograph. Densitometric measurement was performed by imageJ software (NIH, MD, USA). Integrated optical density (IOD) of all the positive staining of STYX in each photograph was measured, and its ratio to total area of each photograph was calculated as STYX density [24]. FBXW7 density was calculated by the same method. The optimal cutoff-point of STYX or FBXW7 density was obtained with X-TILE 3.6.1 software (Yale University, CT, USA), as described previously [25].

2.3. Cell proliferation and colony formation assay

Cell viability was tested by the cell counting kit (CCK)-8 assay (Dojindo, Tokyo, Japan) as previously reported [26]. For the colony formation assay, 1×10^3 cells/per well were incubated in 6-well plates. After 12 days, the visible colonies were fixed with 4% formaldehyde and stained with crystal violet. Colonies containing more than 50 cells were counted.

2.4. Apoptosis assay

In vitro and *in vivo* apoptosis assays were assessed by flow cytometry (BD Biosciences, CA, USA) and TUNEL (Promega, WI, USA) experiment, respectively, as previously described [27,28].

2.5. Migration and invasion assay

Cell migration and invasion assays were performed using transwell plates (8-μm pore size; Corning, 3422). Briefly, 3×10^5 cells/well were resuspended with serum-free medium in the top chamber of the transwell plates coated with or without Matrigel (BD, 356234), and medium with 10% FBS was added to the bottom chamber. After 24 h, the cells that had migrated across the membrane were fixed with 4% paraformaldehyde, stained with crystal violet. Migrated or invaded Cells were counted by three randomly selected fields with a microscope (Olympus Corporation, Tokyo, Japan) under 200 × magnification.

Table 2
Multivariate Cox regression analysis for the overall survival and disease-free survival of 140 CRC patients.

Variables	Overall survival		Disease-free survival	
	P value	HR (95%CI)	*P* value	HR (95%CI)
Tumor size	0.365	0.786 (0.467–1.323)	0.192	0.742 (0.475–1.161)
Invasive depth	0.508	0.804 (0.421–1.535)	0.929	1.027 (0.568–1.859)
Lymph node metastasis	0.027*	1.998 (1.081–3.693)	0.001*	2.587 (1.491–4.489)
Distant metastasis	0.000*	9.770 (4.617–20.675)	0.000*	8.648 (4.213–17.751)
TNM stage	0.052	1.820 (0. 996–3.328)	0.003*	2.277 (1.331–3.894)
STYX expression	0.009*	2.324 (1.235–4.373)	0.047*	1.678 (1.006–2.799)

* Statistically significant.

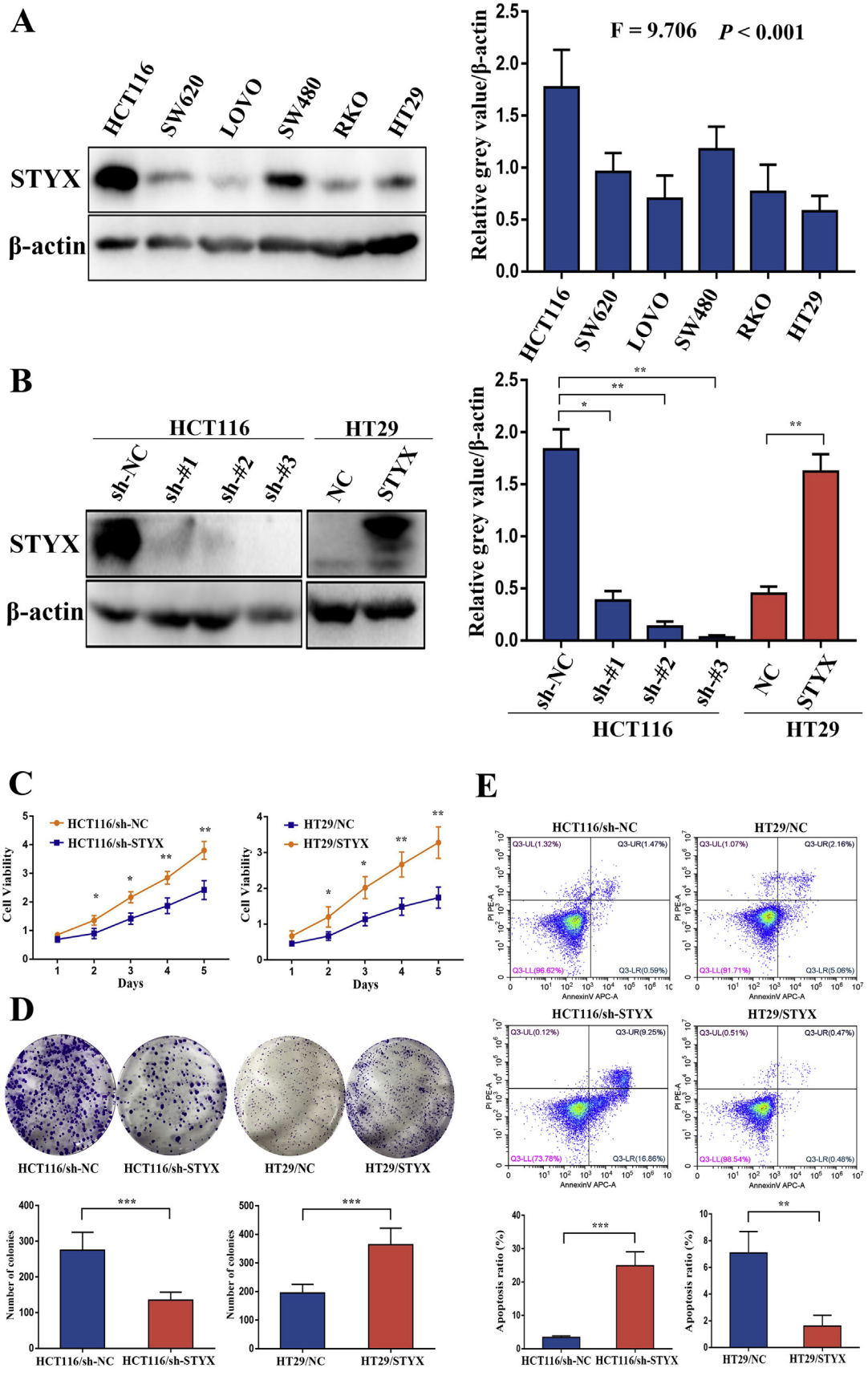

Fig. 2. STYX promoted cell proliferation, colony formation, and inhibited apoptosis in CRC cells. (A) STYX expression in six CRC cell lines as detected by Western blot analysis. (B) STYX knockdown and overexpression as detected by Western blot. (C) Viability of STYX-silenced or STYX-overexpressed CRC cells as detected by the CCK-8 assay. (D) Colony-formation ability of STYX-silenced or STYX-overexpressed CRC cells as detected by the colony formation assay. (E) Apoptosis of STYX-silenced or STYX-overexpressed CRC cells as detected by flow cytometry. Results represent means ± SD from three independent experiments. $^{*}P < 0.05$, $^{**}P < 0.01$.

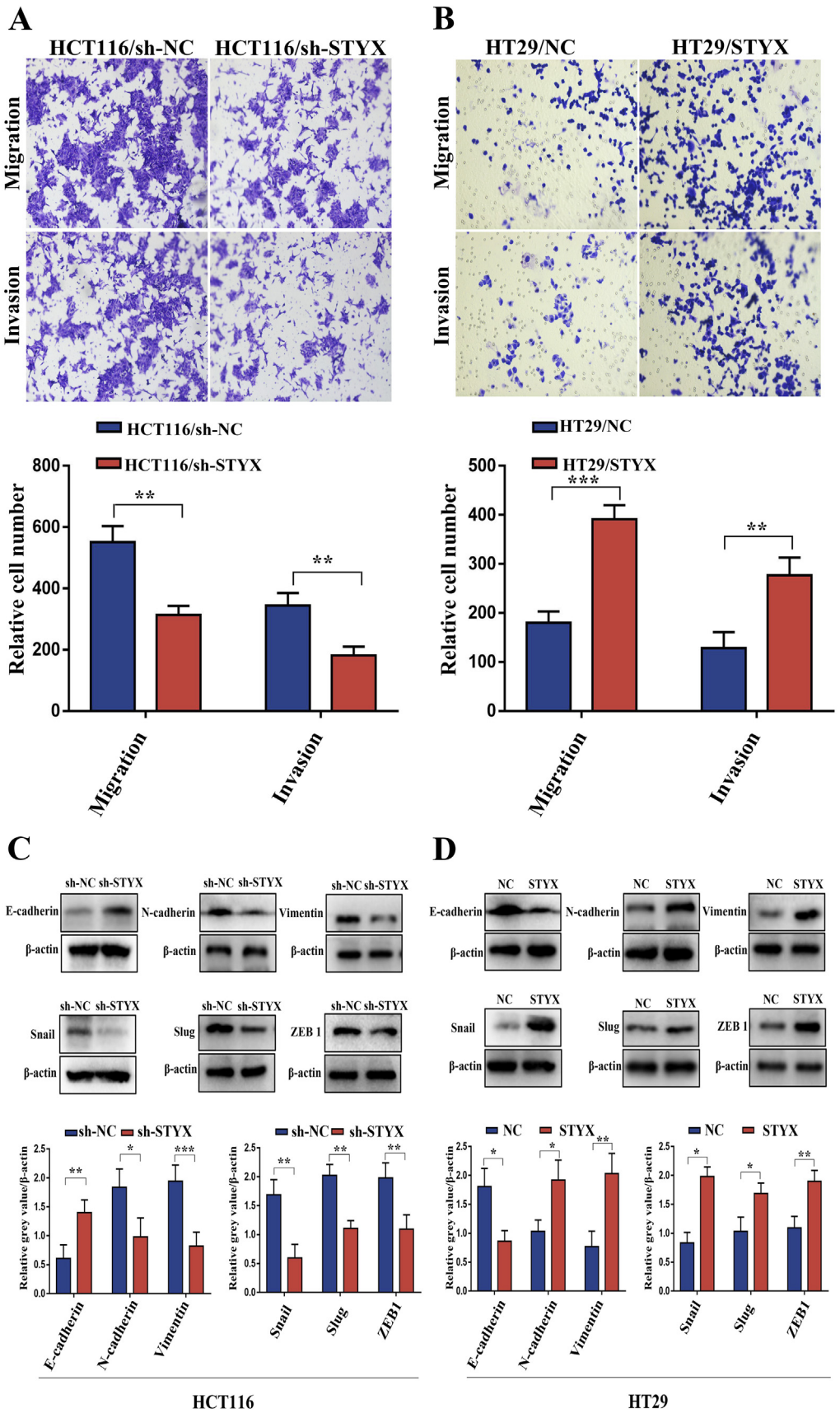

Fig. 3. STYX contributed to cell migration, invasion, and EMT in CRC cells. (A) Transwell Matrigel invasion and migration assay for STYX-silenced HCT116 cells. (B) Transwell Matrigel invasion and migration assay for STYX-overexpressed HT29 cells. (C) EMT marker expression in STYX-silenced HCT116 cells as detected by Western blot analysis. (D) EMT marker expression in STYX-overexpressed HT29 cells as detected by Western blot analysis. Results represent means ± SD from three independent experiments. $^{*}P < 0.05$, $^{**}P < 0.01$, $^{***}P < 0.001$.

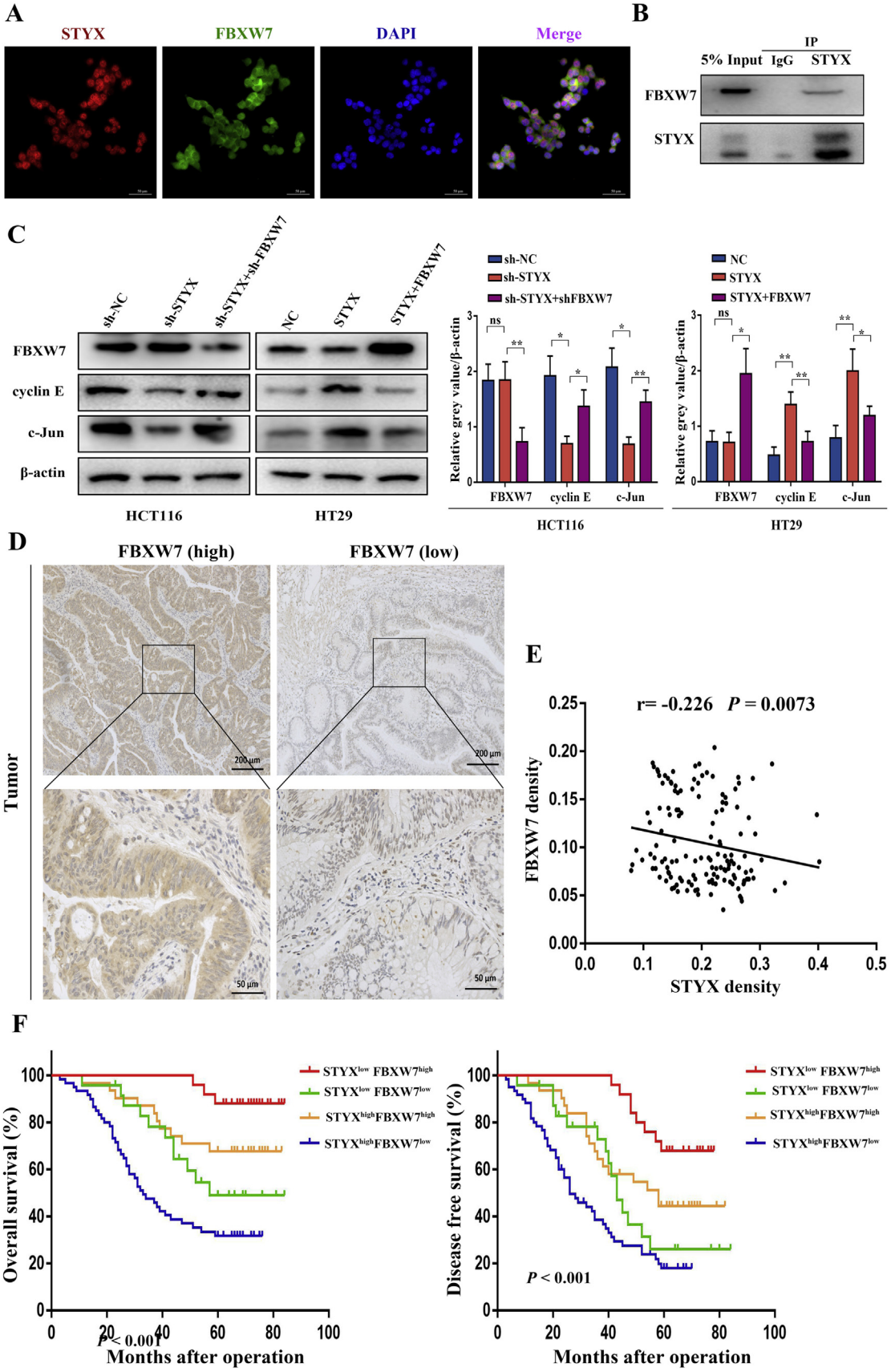

Fig. 4. STYX bound to FBXW7 in CRC cells and negatively correlated with FBXW7 in CRC tissues. (A) Cellular co-localization of STYX and FBXW7 is validated by immunofluorescence in HCT116 cells. (B) Interaction of STYX and FBXW7 was validated by co-immunoprecipitation in HCT116 cells. (C) The expression of FBXW7, cyclin E, and c-Jun in CRC cells as detected by Western blot assay. (D) Representative images of FBXW7 expression in CRC tissues tested by immunohistochemistry. (E) The relationship between the expression of STYX and FBXW7 in CRC tissues analyzed by Pearson's correlation analysis. (F) Kaplan–Meier survival analysis according to the combination of STYX and FBXW7 expression in 140 CRC patients. $^{ns}P > 0.05$, $^{*}P < 0.05$, $^{**}P < 0.01$.

Table 3
Relationship between the STYX-FBXW7 expression levels, TNM stages and prognosis.

Groups	Case	TNM stages		*P* value	5-year OS (%)	*P* value	5-year DFS (%)	*P* value
	(n = 140)	I + II	III + IV					
				0.002*		< 0.001*		< 0.001*
$STYX^{high}FBXW7^{low}$	60	11 (18.3%)	49 (81.7%)		31.67		17.89	
$STYX^{high}FBXW7^{high}$	31	13 (41.9%)	18 (58.1%)		67.04		44.4	
$STYX^{low}FBXW7^{high}$	25	15 (60%)	10 (40%)		88		68	
$STYX^{low}FBXW7^{low}$	24	9 (37.5%)	15 (62.5%)		49.02		26.06	

* Statistically significant.

2.6. Western blot (WB) and co-immunoprecipitation (co-IP)

Total cellular proteins were extracted using lysis buffer containing phenylmethylsulfonyl fluoride (PMSF) and phosphatase inhibitor. Equal amounts (30 μg) of total protein from various samples were separated via SDS–PAGE and transferred to PVDF membranes, which were blocked with 5% skimmed milk in TBST for 1 h, and incubated overnight at 4 °C with the various primary antibodies. The membranes were then incubated with secondary antibody (CST, MA, USA) for 1 h at room temperature. Protein visualization was performed using a chemiluminescence kit (Beyotime Biotechnology, China). The primary antibodies used are listed as follows: STYX (1:1000; Abcam, USA); FBXW7 (1:1000; Abcam, USA); Cyclin E (1:1000; Abcam, USA); c-Jun (1:1000; Abcam, USA); E-cadherin (1:5000; Abcam, USA); N-cadherin (1:5000; Abcam, MA, USA); Vimentin (1:1000; Abcam, MA, USA); Snail (1:1000; Abcam, MA, USA); Slug (1:1000; CST, MA, USA); ZEB1 (1:1000; Abcam, MA, USA); and β-actin (1:2000; CST, MA, USA).

RIPA lysis buffer was used to obtain total protein lysates from cells. Primary antibody (4 μg) was added into 1000 μg of total protein, and then the mixture was incubated on a rotary shaker at 4 °C overnight. The protein A Sepharose beads (Santa Cruz, Texas, USA) were added to the mixture and rotated at 4 °C for 1 h. The beads were collected by centrifugation for 3 min at 800 g. Subsequently, 2 × sample loading buffer was used to resuspend the Sepharose beads–antigen–antibody complexes. The samples were collected for the WB assay after boiling for 5 min with the sample-loading buffer.

2.7. Immunofluorescence (IF)

The cells were seeded on glass coverslips for 24 h, fixed with 4% paraformaldehyde for 10 min, and permeabilized in 0.25% Triton X-100 (ZSGB-Bio, Beijing, China) for 10 min. The cells were then blocked with 5% BSA in PBS for 30 min at room temperature and incubated in antibodies overnight at 4 °C. Following this, the cells were incubated in Alexa Fluor 488 Goat anti-rabbit IgG and Alexa Fluor 647 Donkey anti-mouse IgG (each, 1:500, Abcam, USA) secondary antibodies for 1 h at room temperature. The nuclei were counterstained with DAPI (Thermo, MA, USA) for 30 min. Fluorescence images were captured using a fluorescence microscope (Olympus Corporation, Tokyo, Japan).

2.8. In vivo models

Male BALB/c nude mice (6-week-old) were purchased from the Experimental Animal Center of the Sichuan University and housed in SPF conditions. All animal care and handling procedures were performed in accordance with the National Institutes of Health guide for the care and use of Laboratory animals and approved by the Animal Care and Use Committee of West China Hospital, Sichuan University.

For the tumor growth model, 3×10^6 cells (two groups including HT29-vector cells and HT29-STYX cells) were subcutaneously injected into the right flanks. Tumor volume was measured with calipers every 7 days and calculated using the formula: Volume (mm^3) = length × $width^2/2$. All mice were sacrificed 5 weeks post-injection, and tumor growth and apoptosis analyzed by IHC and TUNEL staining.

For the tumor metastasis model [29], HT29 cells were transfected with PGKV5-luciferase vector and treated with G418 at 4 μg/mL to obtain a cell line stably expressing luciferase, which was treated with control or STYX to generate two groups. Each mouse was injected with 1×10^6 cells in 100 μL PBS by the tail-vein. After 5 weeks, the mice were anesthetized with 3% isoflurane, intraperitoneally injected with luciferin (300 mg/kg, 10 min prior to imaging), and imaged in an IVIS spectrum imaging system (Caliper, Newton, USA). The images were analyzed using the Living Image software (Caliper, Newton, USA). Post-imaging, the mice were sacrificed, and the lungs were removed for H&E staining.

2.9. Statistical analysis

The χ^2 test or Fisher's exact test was used to analyze the correlation between STYX expression and the clinicopathological features of CRC patients. The Kaplan-Meier method was used to analyze patient survival. The Student's *t*-test was used to analyze the comparisons between the two groups. Cox regression model was used in multivariate analysis to study the effectors of clinical variables on survival. Statistical analysis and graphs were generated using the SPSS 20.0 software program and the GraphPad Prism 7 software. $P < 0.05$ were considered significant.

3. Results

3.1. STYX expression was significantly associated with clinicopathological characteristics and predicted prognosis in CRC patients

We first performed WB to examine the expression levels of STYX in 20 CRC tissues. As shown in Fig. 1A and Supplementary Fig. S1, STYX expression levels were markedly increased in tumor tissues compared to that in matched normal tissues ($P < 0.05$). To investigate the clinical significance of STYX expression in CRC, we further evaluated STYX protein expression in 140 pairs of tumor tissues and matched normal tissues by IHC. The results showed increased expression of STYX in the tumor tissues compared with matched normal tissues (Fig. 1B and Supplementary Fig. S2). Further, STYX expression significantly correlated with tumor size ($P = 0.046$), invasive depth ($P = 0.034$), lymph node metastasis ($P = 0.017$), and TNM stages ($P = 0.009$), but not to age, gender, and location ($P > 0.05$, Table 1). Moreover, Kaplan–Meier analysis showed that patients with high STYX expression (n = 91) had a significantly poorer 5-year overall survival (OS) than those with low STYX expression (n = 49; log-rank = 10.56; $P = 0.0012$; Fig. 1C). High STYX expression was associated with a shorter disease-free survival (DFS) time compared to low STYX expression (log rank = 10.79, $P = 0.0010$, Fig. 1C). Further, multivariate COX regression analysis showed that STYX expression independently predicted patient OS ($P = 0.009$, HR 2.324, 95% CI 1.235–4.373) and DFS ($P = 0.047$, HR 1.678, 95% CI 1.006–2.799; Table 2). These findings indicated that STYX might be a potential prognostic marker in

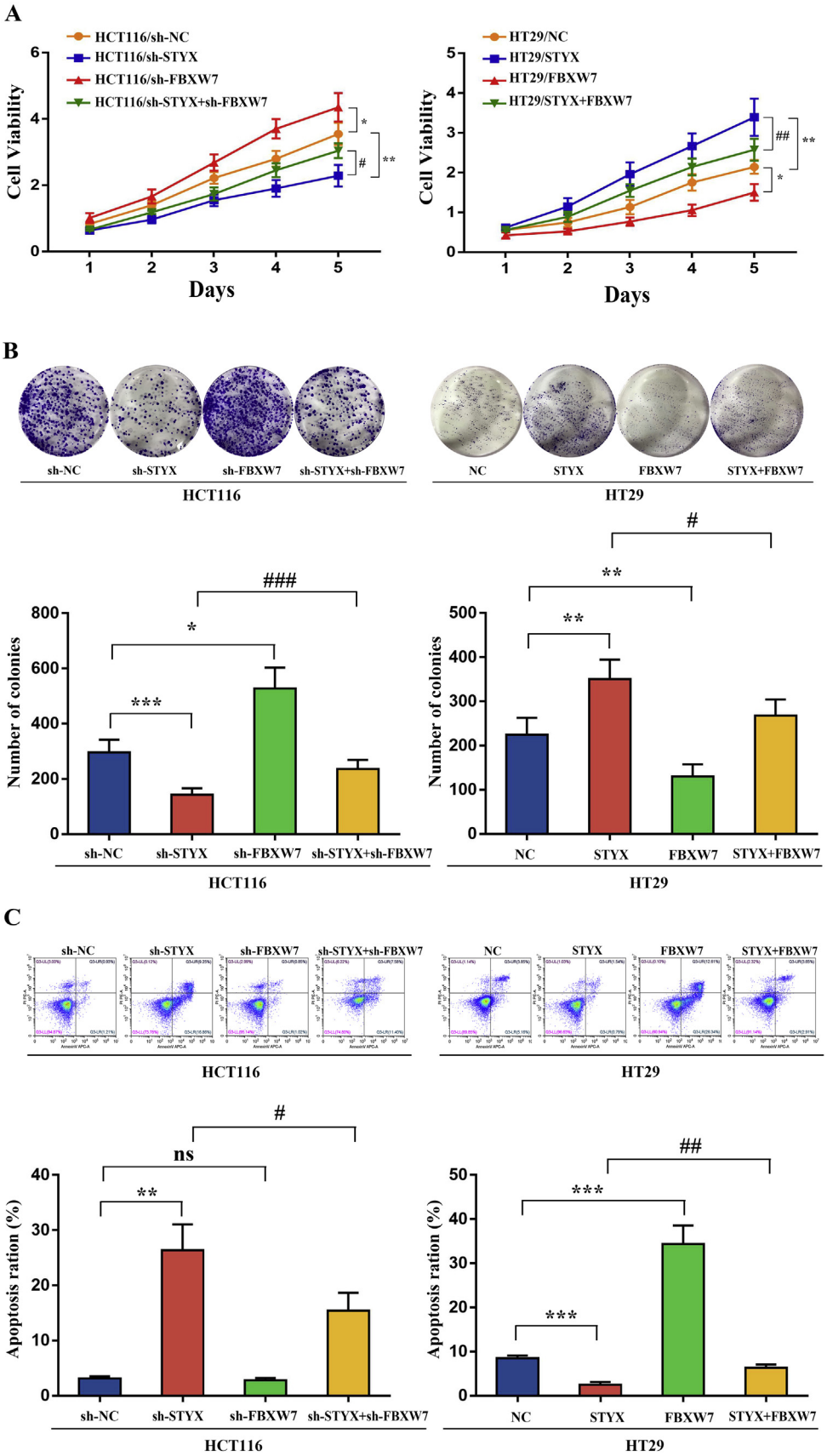

Fig. 5. STYX promoted CRC cell proliferation, colony-formation ability, and inhibited apoptosis by targeting FBXW7. (A) Cell viability of HCT116 cells and HT29 cells with co-regulation of STYX and/or FBXW7 tested by the CCK-8 assay. (B) Colony-formation ability of HCT116 cells and HT29 cells with co-regulation of STYX and/or FBXW7 detected by the colon formation assay. (C) Apoptosis of HCT116 cells and HT29 cells with co-regulation of STYX and/or FBXW7 tested by the flow cytometry. Results represent means ± SD from three independent experiments. $^{ns}P > 0.05$, $^{*}P < 0.05$, $^{**}P < 0.01$, $^{***}P < 0.001$; $^{\#}P < 0.05$, $^{\#\#}P < 0.01$, $^{\#\#\#}P < 0.001$.

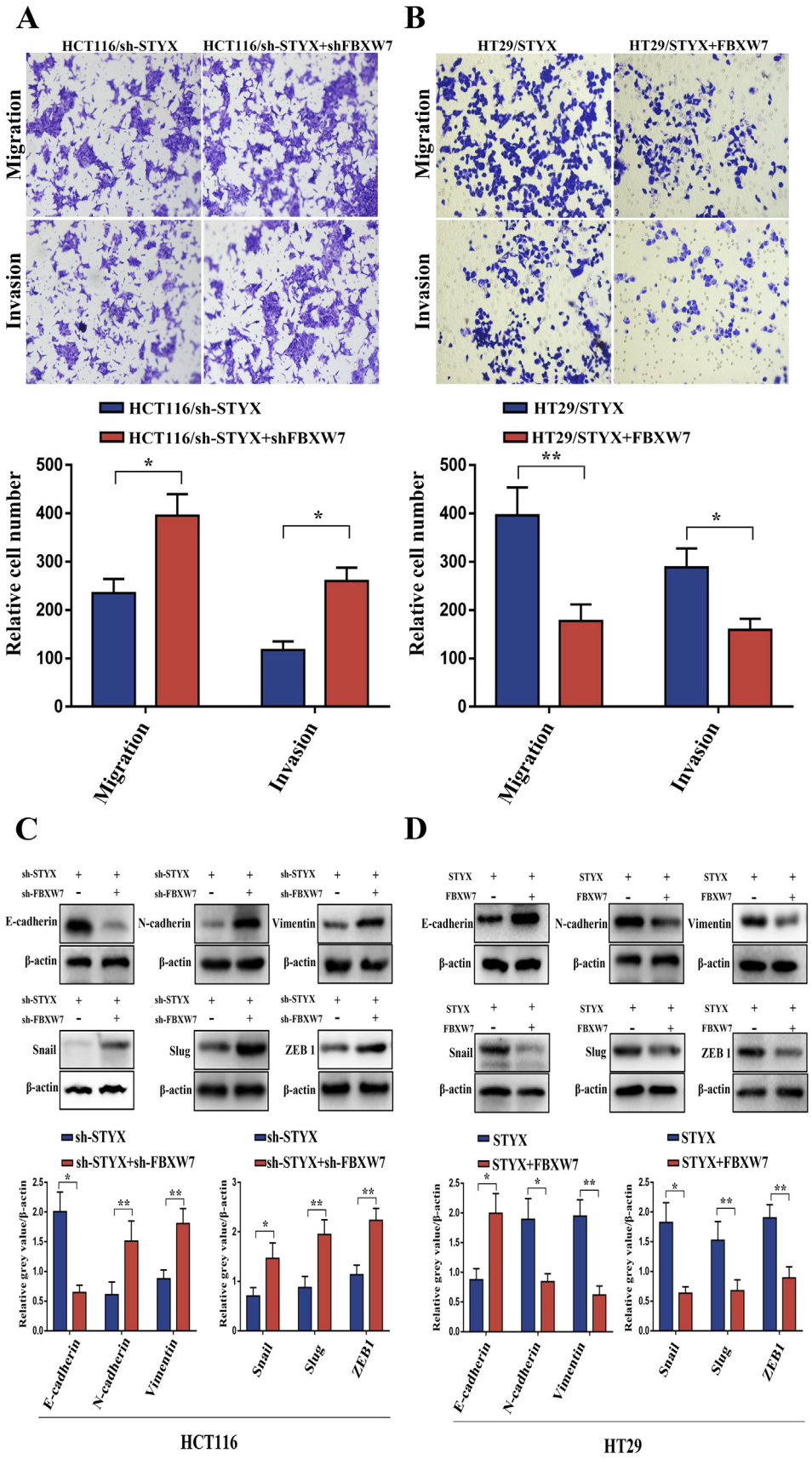

Fig. 6. STYX promoted CRC cell migration, invasion, and EMT by targeting FBXW7. (A) Transwell Matrigel invasion and migration assay for HCT116 cells with co-depletion of STYX and FBXW7. (B) Transwell Matrigel invasion and migration assay for HT29 cells with co-overexpression of STYX and FBXW7. (C) EMT marker expression in HCT116 cells with co-depletion of STYX and FBXW7 as detected by Western blot analysis. (D) EMT marker expression in HT29 cells with co-overexpression of STYX and FBXW7 as detected by Western blot analysis. Results represent means ± SD from three independent experiments. $^{*}P < 0.05$, $^{**}P < 0.01$, $^{***}P < 0.001$.

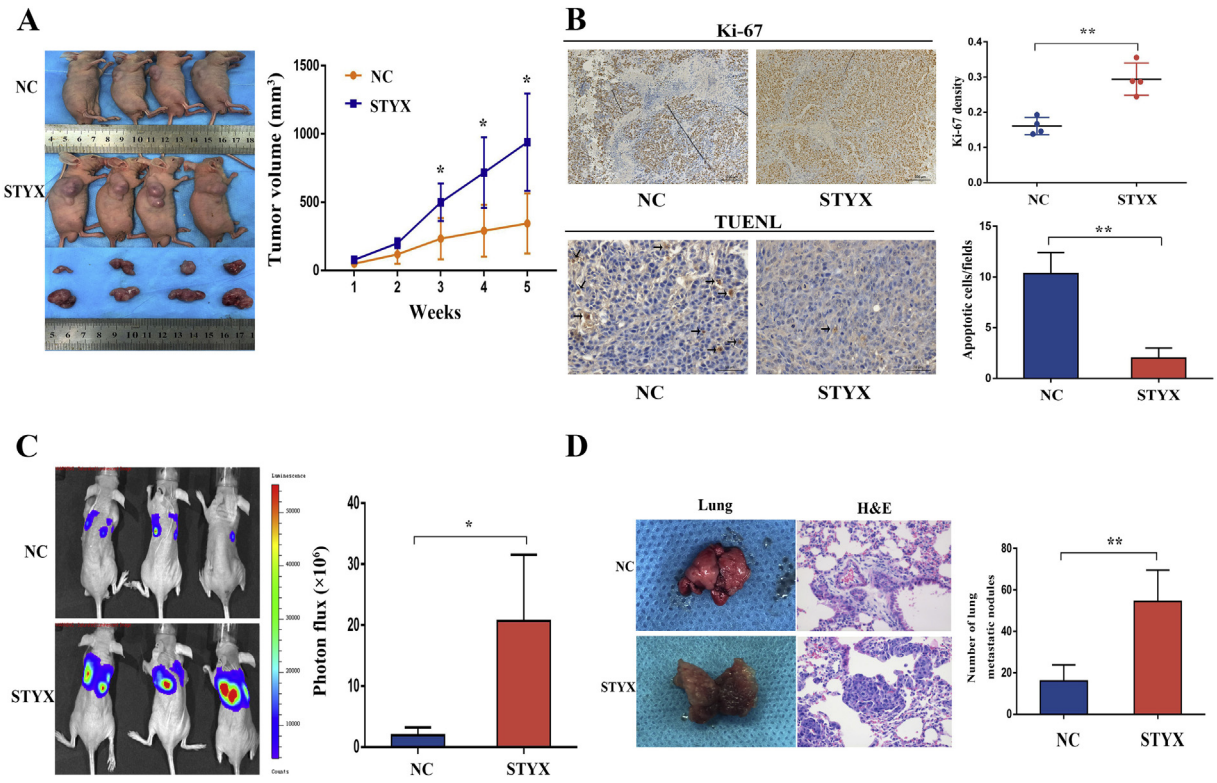

Fig. 7. Overexpression of STYX promoted tumor growth and metastasis *in vivo*. (A) Effects of STYX overexpression on tumor growth *in vivo* (B) Representative images of Ki-67 expression in xenograft tested by immunohistochemistry. The apoptosis was assessed by TUNEL assays. (C) Effects of STYX overexpression on lung tumor metastasis detected by bioluminescent images of whole mouse bodies. (D) Representative images of lung metastasis were obtained 5 weeks after injection. Results represent means ± SD from three independent experiments. $^{*}P < 0.05$, $^{**}P < 0.01$.

CRC.

3.2. STYX promoted proliferation, colony-formation ability, and inhibited apoptosis in CRC cells

To explore the influence of STYX on the biological behaviors of CRC, we applied lentiviral transfection technique to regulate the expression of STYX in CRC cells. We first quantified the expression levels of STYX in 6 CRC cell lines. As shown in Fig. 2A, STYX was especially high in HCT116 cells, but low in HT29 cells. Therefore, HCT116 cells were transduced with STYX-shRNA to knockdown STYX, and HT29 cells were transduced with STYX to overexpress STYX. Control cells were transduced with negative control viruses. All these stable transfected cells were tested regularly by WB to confirm the efficiency of down-regulation or up-regulation. As shown in Fig. 2B, shRNA#3 showed the strongest efficiency of knockdown and was used for further research.

The effects of STYX on viability, colony-formation ability and apoptosis of CRC cells were analyzed by CCK-8 assay, colony formation assay and flow cytometry, respectively. As shown in Fig. 2C, STYX knockdown significantly decreased the viability of HCT116 cells whereas STYX overexpression increased the viability of HT29 cells. Moreover, the results of the colony formation assay were in accord with results from the CCK-8 assay (Fig. 2D). Flow cytometry analysis showed that STYX knockdown enhanced the apoptotic rate of HCT116 cells, whereas overexpression reduced the apoptotic rate of HT29 cells (Fig. 2E). Therefore, we concluded that STYX promoted proliferation and colony-formation ability, and inhibited apoptosis in CRC cells.

3.3. STYX promoted migration, invasion, and epithelial-mesenchymal transition (EMT) in CRC cells

The effects of STYX on migration and invasion in CRC cells were demonstrated using the Transwell migration and Matrigel invasion assays, respectively. As shown in Fig. 3A, suppression of STYX resulted in significantly diminished migratory and invasive potential in HCT116 cells. Conversely, a marked increase of cell migration and invasion ability was observed in HT29 cells with elevated STYX expression (Fig. 3B). These data suggested that STYX facilitated CRC cell migration and invasion.

Given the crucial role of EMT in tumor metastasis [30–33], we evaluated the protein levels of EMT markers including E-cadherin, N-cadherin and Vimentin, and a panel of EMT-associated transcription factors including Snail, Slug, and ZEB1 in HCT116 and HT29 cells. Knockdown of STYX in HCT116 cells led to significantly higher levels of E-cadherin and lower levels of N-cadherin, Vimentin, Snail, Slug, and ZEB1 (Fig. 3C). In contrast, the enhanced expression of STYX in HT29 cells resulted in a concomitant up-regulation of N-cadherin, Vimentin, Snail, Slug, and ZEB1, accompanied by reduction of E-cadherin (Fig. 3D). These data led us to the conclusion that STYX might induce the EMT in CRC cells.

3.4. STYX interacted with FBXW7 and regulated its function in CRC cells

To investigate the relationship between STYX and FBXW7 in CRC cells, we first performed IF and co-IP experiments. The cellular co-localization of STYX and FBXW7 proteins was shown by IF in HCT116 cells (Fig. 4A). The co-IP results showed that endogenous STYX interacted with FBXW7 in HCT116 cells (Fig. 4B). Then, WB was used to explore the effects of altering STYX levels on FBXW7 expression. As shown in Fig. 4C, FBXW7 expression level was changed neither in the STYX-silenced HCT116 cells nor in STYX-overexpressed HT29 cells compared with the negative control cells ($P > 0.05$, respectively). Moreover, knockdown or overexpression of STYX resulted in a drop or rise in the expression levels of cyclin E and c-Jun, which are substrates

of FBXW7 (Fig. 4C). In addition, co-depletion of both STYX and FBXW7 enhanced the levels of cyclin E and c-Jun compared to depletion of STYX alone (Fig. 4C). Co-overexpression of both STYX and FBXW7 reduced the levels of cyclin E and c-Jun compared with overexpression of STYX alone (Fig. 4C). These results suggested that the effects of STYX on the expression levels of cyclin E and c-Jun depended on FBXW7, and further indicated that STYX regulated FBXW7 function rather than FBXW7 expression in CRC cells.

3.5. Expression of STYX and FBXW7 were inversely correlated in CRC tissues

We then analyzed the relationship between the expression of FBXW7 and STYX in our cohort of 140 CRC cases. Representative images of FBXW7 staining are shown in Fig. 4D. The expression of FBXW7 in cancer tissues was lower than that in paired normal tissues. ($P = 0.001$, Supplementary Fig. S3), which correlated to the prognosis of CRC patients (Supplementary Fig. S4). Pearson's correlation analysis revealed a strong negative correlation between the expression of FBXW7 and STYX ($r = -0.226$, $P < 0.01$, Fig. 4E). In addition, patients with low STYX accompanying high FBXW7 expression exhibited the best prognoses and highest proportion of stage (I + II), whereas patients with high STYX accompanying low FBXW7 expression exhibited the worst prognoses and highest proportion of stage (III + IV) (Fig. 4F, Table 3).

3.6. STYX regulated CRC cell proliferation, colony-formation ability, and apoptosis, by targeting FBXW7

To investigate whether FBXW7 mediated the influence of STYX on the biological behaviors of CRC cells, we established the co-depletion of both STYX and FBXW7 HCT116 cells, and the co-overexpression of both STYX and FBXW7 HT29 cells. As shown in Fig. 5A and B, depletion of STYX significantly decreased the cell viability and colony-formation ability of HCT116 cells, while depletion of FBXW7 significantly increased the cell viability and colony-formation ability of HCT116 cells. Compared with depletion of STYX alone, co-depletion of both STYX and FBXW7 restored cell viability and colony-formation ability back near to control cells (Fig. 5A and B). As shown in Fig. 5C, depletion of STYX increased cell apoptosis of HCT116 cells. Compared with depletion of STYX alone, co-depletion of both STYX and FBXW7 restored cell apoptosis back near to control cells (Fig. 5C). The overexpression of STYX and/or FBXW7 resulted in effects opposite to these observations in HT29 cells (Fig. 5A–C). These results demonstrated that STYX regulated CRC cell proliferation, colony-formation, and apoptosis by targeting FBXW7.

3.7. STYX regulated CRC cell migration, invasion, and EMT by targeting FBXW7

As shown in Fig. 6A, co-depletion of both STYX and FBXW7 promoted cell migration and invasion of HCT116 cells compared with depletion of STYX alone. Inversely, co-overexpression of both STYX and FBXW7 suppressed the cell migration and invasion of HT29 cells compared with overexpression of STYX alone (Fig. 6B). WB results revealed that co-depletion of both STYX and FBXW7 increased the levels of Snail, slug, ZEB1, N-cadherin, and Vimentin, and decreased E-cadherin levels in HCT116 cells (Fig. 6C). Co-overexpression of both STYX and FBXW7 yielded the opposite effects in HT29 cells (Fig. 6D). These data indicated that STYX regulated CRC cell migration, invasion, and EMT by targeting FBXW7.

3.8. STYX promoted CRC growth and metastasis in vivo

The data above demonstrated that STYX promotes CRC cell proliferation, migration and invasion. We then examined the effects of STYX on tumorigenesis *in vivo* by injecting control or STYX-overexpressed HT29 cells subcutaneously into the right flank of nude mice. As shown in Fig. 7A, the xenografts in the STYX group grew faster ($P < 0.05$) than those in the NC group. Moreover, compared with the NC group, Ki-67 expression was increased in the STYX group with a corresponding decrease in the number of apoptotic cells (Fig. 7B).

To explore the effects of STYX on CRC metastasis *in vivo*, luciferase-labeled control or STYX-overexpressed HT29 cells were injected into nude mice via the tail vein. After 5 weeks, whole-body luminescence signals in the STYX group were ~10-fold higher than those in the NC group ($P < 0.05$, Fig. 7C). Further, H&E staining revealed that STYX-overexpressed HT29 cells formed more nodules in the lungs that were also larger than those in the control cell-injected animals (Fig. 7D). Together, these data strongly indicated that STYX promoted CRC growth and metastasis *in vivo*.

4. Discussion

In the present study, we found that the CRC tissues overexpressed STYX in comparison with the matched normal tissues, which positively correlated with tumor size, tumor invasive depth, lymph node metastasis, and TNM stages. Kaplan–Meier and multivariate COX regression analysis revealed that the high expression of STYX was independently related to a poorer 5-year OS and DFS of CRC patients. To the best of our knowledge, this is the first study to reveal the expression level of STYX and its relation with the clinicopathological features and prognosis of patients with CRC. The results indicated that STYX may play a role as a promoter in the development of CRC, and is a valuable prognostic biomarker for CRC. Consistent with our findings, STYX upregulation in breast cancer was related to poor patient prognosis, implying its oncogenic role [10].

To date, there is no study that reports the effects of STYX on CRC cells, but previous studies have consistently demonstrated that it plays an oncogenic role in other tumors, including inhibiting apoptosis of breast cancer cells and promoting cell migration of Hela cells [9,10]. In the present study, various lines of evidence indicated that STYX knockdown reduced aggressiveness and malignancy of HCT116 cells, with a higher ratio of apoptosis and a reduction in *in vitro* cell proliferation and colony-formation ability. Moreover, STYX knockdown led to a reduction in *in vitro* cell migration and invasion. In contrast, overexpression of STYX had the opposite effects on HT29 cells and promoted *in vivo* tumor growth and lung metastasis. These results demonstrated that STYX facilitated tumor growth and metastasis by enhancing the aggressiveness and malignancy of CRC cells and is therefore an oncogene in CRC.

The EMT process is a major factor resulting in the metastasis of various cancers including CRC [34–36]. During this process, cells lose epithelial characteristics including decreased E-cadherin expression and acquire mesenchymal features such as an increase in N-cadherin and Vimentin expression [37]. The proteins Snail, Slug, and ZEB1 play key roles in EMT as upstream transcription factors [30,31]. The present study revealed that depletion of STYX enhanced E-cadherin expression, with a concomitant reduction in the expression of the mesenchymal markers N-cadherin and Vimentin, and that of the transcription factors Snail, slug, and ZEB1. Overexpression of STYX had the reverse effects on expression of these proteins. These results indicated that STYX facilitated EMT by up-regulating Snail, slug, and ZEB1. Therefore, regulation of EMT may be one of the mechanisms by which STYX promotes CRC metastasis.

FBXW7 represents a general tumor suppressor in various cancers by targeting several important oncoproteins, such as cyclin E [38], c-Jun [39], c-Myc [40], and Notch [41]. Many oncogenes are reported to promote the development of tumors by regulating FBXW7. Previous studies mainly focused on the regulation of FBXW7 expression by microRNAs, regulation of FBXW7 dimerization, or the phosphorylation of its substrates [42–44]. In the present study, several lines of evidence

suggested that STYX inhibits FBXW7 function by direct protein-protein interaction without influencing its expression in CRC cells: (1) STYX and FBXW7 were co-localized and interacted in the nucleus of CRC cells. (2) Depletion or overexpression of STYX did not alter FBXW7 expression, but significantly down or up-regulated the expression of substrates of FBXW7, cyclin E, and c-Jun. (3) Co-regulation of STYX and FBXW7 expression reversed the changes in expression of cyclin E and c-Jun mediated by regulation of STYX alone. Further, we speculated that the effects of STYX on CRC cells might be associated with the dysfunction of FBXW7 protein. To confirm this hypothesis, we explored the effects of co-regulation of STYX and FBXW7 expression on the biological behaviors of CRC cells. As expected, co-regulation of both STYX and FBXW7 expression reversed the biological changes of CRC cells mediated by regulation of STYX expression alone, implying FBXW7 might be involved in STYX-modulated biological behaviors and could be a critical target of STYX in CRC cells. Thus, we concluded that the biological impact of STYX on CRC cells was achieved by regulating FBXW7.

Furthermore, we integrated the expression information of STYX and FBXW7 to analyze the significance in prognosis prediction. As seen in Table 3, patients with high STYX accompanying low FBXW7 expression had the highest proportion of stage (III + IV) cases and worst 5-year OS and DFS. Conversely, patients expressing low STYX accompanying high FBXW7 had the highest proportion of stage (I + II) and best 5-year OS and DFS. The results strongly demonstrated that the combination of STYX and FBXW7 expression could provide more accurate information in predicting the tumor stage and prognosis, thus representing a promising biomarker. The findings were consistent with the functions of the two genes in CRC, as shown in the present study.

The main limitation of this study is the relatively small number of CRC patients, which may compromise the reliability of some results. For example, *in vivo* experiments showed a promoting role of STYX in lung metastasis, but the analysis of clinicopathological features did not show a significant relation between STYX expression and distant metastasis for CRC patients. The lack of correlation between STYX expression and distant metastasis may be explained by the relatively small number of samples, which has confined the statistical significance.

In conclusion, this is the first study to identify the clinical significance of STYX in CRC through analyzing the relationship between STYX expression and prognosis of CRC patients and to delineate its effects on the biological behaviors of CRC and the underlying mechanism. Our study strongly suggests that STYX promotes CRC growth and metastasis by modulating the activity of FBXW7. These findings point out a potential role of STYX in the development of CRC, which might represent a novel prognostic biomarker and a promising therapeutic target for CRC. Future studies may be needed to identify small molecular compounds that prevent STYX from binding to FBXW7, thereby rescuing FBXW7 from inhibition and restoring its tumor suppressor effects.

Conflicts of interest statement

The authors declare no conflict of interest.

Acknowledgements

The authors thank Ms. Zhao Xue (Department of Foreign Languages, Sichuan University, China) and Dr. Ailsa Jeffries (Dana-Farber Cancer Institute, USA) for polishing this manuscript. The authors thank Elsevier Publisher for their assistance of language editing. This study was supported by National Natural Science Foundation of China [grant numbers 81472304]; National Key Research and Development Program of China [grant numbers 2016YFC0906000 [2016YFC0906003]]; Sichuan Science and Technology Program [grant numbers 2017JY0020]; and 1.3.5 project for disciplines of excellence, West China Hospital, Sichuan University.

Appendix A. Supplementary data

Supplementary data to this article can be found online at https://doi.org/10.1016/j.canlet.2019.04.014.

References

[1] R. Siegel, D. Naishadham, A. Jemal, Cancer statistics, CA A Cancer J. Clin. 63 (2013) 11–30 2013.
[2] L.A. Torre, F. Bray, R.L. Siegel, J. Ferlay, J. Lortet-Tieulent, A. Jemal, Global cancer statistics, CA A Cancer J. Clin. 65 (2012) 87–108 2015.
[3] R.L. Siegel, K.D. Miller, S.A. Fedewa, D.J. Ahnen, R.G.S. Meester, A. Barzi, A. Jemal, Colorectal cancer statistics, CA A Cancer J. Clin. 67 (2017) 177–193 2017.
[4] W. De Roock, V. De Vriendt, N. Normanno, F. Ciardiello, S. Tejpar, KRAS, BRAF, PIK3CA, and PTEN mutations: implications for targeted therapies in metastatic colorectal cancer, Lancet Oncol. 12 (2011) 594–603.
[5] M.J. Wishart, J.E. Dixon, Gathering STYX: phosphatase-like form predicts functions for unique protein-interaction domains, Trends Biochem. Sci. 23 (1998) 301–306.
[6] M.J. Wishart, J.M. Denu, J.A. Williams, J.E. Dixon, A single mutation converts a novel phosphotyrosine binding domain into a dual-specificity phosphatase, J. Biol. Chem. 270 (1995) 26782–26785.
[7] M. Uhlen, L. Fagerberg, B.M. Hallstrom, C. Lindskog, P. Oksvold, A. Mardinoglu, A. Sivertsson, C. Kampf, E. Sjostedt, A. Asplund, I. Olsson, K. Edlund, E. Lundberg, S. Navani, C.A. Szigyarto, J. Odeberg, D. Djureinovic, J.O. Takanen, S. Hober, T. Alm, P.H. Edqvist, H. Berling, H. Tegel, J. Mulder, J. Rockberg, P. Nilsson, J.M. Schwenk, M. Hamsten, K. von Feilitzen, M. Forsberg, L. Persson, F. Johansson, M. Zwahlen, G. von Heijne, J. Nielsen, F. Ponten, Proteomics. Tissue-based map of the human proteome, Science 347 (2015) 1260419.
[8] M.J. Wishart, J.E. Dixon, The archetype STYX/dead-phosphatase complexes with a spermatid mRNA-binding protein and is essential for normal sperm production, Proc. Natl. Acad. Sci. U. S. A. 99 (2002) 2112–2117.
[9] V. Reiterer, D. Fey, W. Kolch, B.N. Kholodenko, H. Farhan, Pseudophosphatase STYX modulates cell-fate decisions and cell migration by spatiotemporal regulation of ERK1/2, Proc. Natl. Acad. Sci. U. S. A. 110 (2013) E2934–E2943.
[10] V. Reiterer, C. Figueras-Puig, F. Le Guerroue, S. Confalonieri, M. Vecchi, D. Jalapothu, S.M. Kanse, R.J. Deshaies, P.P. Di Fiore, C. Behrends, H. Farhan, The pseudophosphatase STYX targets the F-box of FBXW7 and inhibits SCFFBXW7 function, EMBO J. 36 (2017) 260–273.
[11] J. Heo, R. Eki, T. Abbas, Deregulation of F-box proteins and its consequence on cancer development, progression and metastasis, Semin. Canc. Biol. 36 (2016) 33–51.
[12] S. Uddin, A.A. Bhat, R. Krishnankutty, F. Mir, M. Kulinski, R.M. Mohammad, Involvement of F-BOX proteins in progression and development of human malignancies, Semin. Canc. Biol. 36 (2016) 18–32.
[13] Z. Wang, H. Inuzuka, J. Zhong, L. Wan, H. Fukushima, F.H. Sarkar, W. Wei, Tumor suppressor functions of FBW7 in cancer development and progression, FEBS Lett. 586 (2012) 1409–1418.
[14] S. Akhoondi, D. Sun, N. von der Lehr, S. Apostolidou, K. Klotz, A. Maljukova, D. Cepeda, H. Fiegl, D. Dafou, C. Marth, E. Mueller-Holzner, M. Corcoran, M. Dagnell, S.Z. Nejad, B.N. Nayer, M.R. Zali, J. Hansson, S. Egyhazi, F. Petersson, P. Sangfelt, H. Nordgren, D. Grander, S.I. Reed, M. Widschwendter, O. Sangfelt, C. Spruck, FBXW7/hCDC4 is a general tumor suppressor in human cancer, Cancer Res. 67 (2007) 9006–9012.
[15] H. Davis, A. Lewis, A. Behrens, I. Tomlinson, Investigation of the atypical FBXW7 mutation spectrum in human tumours by conditional expression of a heterozygous propellor tip missense allele in the mouse intestines, Gut 63 (2014) 792–799.
[16] M. Welcker, B.E. Clurman, FBW7 ubiquitin ligase: a tumour suppressor at the crossroads of cell division, growth and differentiation, Nat. Rev. Canc. 8 (2008) 83–93.
[17] Z. Guo, Y. Zhou, B.M. Evers, Q. Wang, Rictor regulates FBXW7-dependent c-Myc and cyclin E degradation in colorectal cancer cells, Biochem. Biophys. Res. Commun. 418 (2012) 426–432.
[18] H. Rajagopalan, P.V. Jallepalli, C. Rago, V.E. Velculescu, K.W. Kinzler, B. Vogelstein, C. Lengauer, Inactivation of hCDC4 can cause chromosomal instability, Nature 428 (2004) 77–81.
[19] P. Zhan, Y. Wang, S. Zhao, C. Liu, Y. Wang, M. Wen, J.H. Mao, G. Wei, P. Zhang, FBXW7 negatively regulates ENO1 expression and function in colorectal cancer, Lab. Invest. 95 (2015) 995–1004.
[20] R. Babaei-Jadidi, N. Li, A. Saadeddin, B. Spencer-Dene, A. Jandke, B. Muhammad, E.E. Ibrahim, R. Muraleedharan, M. Abuzinadah, H. Davis, A. Lewis, S. Watson, A. Behrens, I. Tomlinson, A.S. Nateri, FBXW7 influences murine intestinal homeostasis and cancer, targeting Notch, Jun, and DEK for degradation, J. Exp. Med. 208 (2011) 295–312.
[21] B. Ou, J. Zhao, S. Guan, X. Wangpu, C. Zhu, Y. Zong, J. Ma, J. Sun, M. Zheng, H. Feng, A. Lu, Plk2 promotes tumor growth and inhibits apoptosis by targeting Fbxw7/Cyclin E in colorectal cancer, Cancer Lett. 380 (2016) 457–466.
[22] M. Iwatsuki, K. Mimori, H. Ishii, T. Yokobori, Y. Takatsuno, T. Sato, H. Toh, I. Onoyama, K.I. Nakayama, H. Baba, M. Mori, Loss of FBXW7, a cell cycle regulating gene, in colorectal cancer: clinical significance, Int. J. Cancer 126 (2010) 1828–1837.
[23] J.M. Drake, N.A. Graham, T. Stoyanova, A. Sedghi, A.S. Goldstein, H. Cai, D.A. Smith, H. Zhang, E. Komisopoulou, J. Huang, T.G. Graeber, O.N. Witte, Oncogene-specific activation of tyrosine kinase networks during prostate cancer progression, Proc. Natl. Acad. Sci. U. S. A. 109 (2012) 1643–1648.

[24] X.D. Zhu, J.B. Zhang, P.Y. Zhuang, H.G. Zhu, W. Zhang, Y.Q. Xiong, W.Z. Wu, L. Wang, Z.Y. Tang, H.C. Sun, High expression of macrophage colony-stimulating factor in peritumoral liver tissue is associated with poor survival after curative resection of hepatocellular carcinoma, J. Clin. Oncol. 26 (2008) 2707–2716.
[25] R.L. Camp, M. Dolled-Filhart, D.L. Rimm, X-tile: a new bio-informatics tool for biomarker assessment and outcome-based cut-point optimization, Clin. Cancer Res. 10 (2004) 7252–7259.
[26] J. Zhao, P. Li, H. Feng, P. Wang, Y. Zong, J. Ma, Z. Zhang, X. Chen, M. Zheng, Z. Zhu, A. Lu, Cadherin-12 contributes to tumorigenicity in colorectal cancer by promoting migration, invasion, adhersion and angiogenesis, J. Transl. Med. 11 (2013) 288.
[27] D. He, Z. Guo, J.L. Pu, D.F. Zheng, X.F. Wei, R. Liu, C.Y. Tang, Z.J. Wu, Resveratrol preconditioning protects hepatocytes against hepatic ischemia reperfusion injury via Toll-like receptor 4/nuclear factor-kappaB signaling pathway in vitro and in vivo, Int. Immunopharmacol. 35 (2016) 201–209.
[28] L. Lin, Y. Fan, F. Gao, L. Jin, D. Li, W. Sun, F. Li, P. Qin, Q. Shi, X. Shi, L. Du, UTMD-promoted Co-delivery of gemcitabine and miR-21 inhibitor by dendrimer-entrapped gold nanoparticles for pancreatic cancer therapy, Theranostics 8 (2018) 1923–1939.
[29] J. Kong, W. Sun, C. Li, L. Wan, S. Wang, Y. Wu, E. Xu, H. Zhang, M. Lai, Long non-coding RNA LINC01133 inhibits epithelial-mesenchymal transition and metastasis in colorectal cancer by interacting with SRSF6, Cancer Lett. 380 (2016) 476–484.
[30] M. Zeisberg, E.G. Neilson, Biomarkers for epithelial-mesenchymal transitions, J. Clin. Investig. 119 (2009) 1429–1437.
[31] J.P. Thiery, J.P. Sleeman, Complex networks orchestrate epithelial-mesenchymal transitions, Nat. Rev. Mol. Cell Biol. 7 (2006) 131–142.
[32] U. Burk, J. Schubert, U. Wellner, O. Schmalhofer, E. Vincan, S. Spaderna, T. Brabletz, A reciprocal repression between ZEB1 and members of the miR-200 family promotes EMT and invasion in cancer cells, EMBO Rep. 9 (2008) 582–589.
[33] H.N. Chen, K. Yuan, N. Xie, K. Wang, Z. Huang, Y. Chen, Q. Dou, M. Wu, E.C. Nice, Z.G. Zhou, C. Huang, PDLIM1 stabilizes the E-cadherin/beta-catenin complex to prevent epithelial-mesenchymal transition and metastatic potential of colorectal cancer cells, Cancer Res. 76 (2016) 1122–1134.
[34] H. Cao, E. Xu, H. Liu, L. Wan, M. Lai, Epithelial-mesenchymal transition in colorectal cancer metastasis: a system review, Pathol. Res. Pract. 211 (2015) 557–569.
[35] J.P. Thiery, H. Acloque, R.Y. Huang, M.A. Nieto, Epithelial-mesenchymal transitions in development and disease, Cell 139 (2009) 871–890.
[36] J.P. Thiery, Epithelial-mesenchymal transitions in tumour progression, Nat. Rev. Canc. 2 (2002) 442–454.
[37] L. Mi, F. Zhu, X. Yang, J. Lu, Y. Zheng, Q. Zhao, X. Wen, A. Lu, M. Wang, M. Zheng, J. Ji, J. Sun, The metastatic suppressor NDRG1 inhibits EMT, migration and invasion through interaction and promotion of caveolin-1 ubiquitylation in human colorectal cancer cells, Oncogene 36 (2017) 4323–4335.
[38] R. Sancho, A. Jandke, H. Davis, M.E. Diefenbacher, I. Tomlinson, A. Behrens, F-box and WD repeat domain-containing 7 regulates intestinal cell lineage commitment and is a haploinsufficient tumor suppressor, Gastroenterology 139 (2010) 929–941.
[39] J. Kurashige, M. Watanabe, M. Iwatsuki, K. Kinoshita, S. Saito, Y. Hiyoshi, H. Kamohara, Y. Baba, K. Mimori, H. Baba, Overexpression of microRNA-223 regulates the ubiquitin ligase FBXW7 in oesophageal squamous cell carcinoma, Br. J. Canc. 106 (2012) 182–188.
[40] C. Kanei-Ishii, T. Nomura, T. Takagi, N. Watanabe, K.I. Nakayama, S. Ishii, Fbxw7 acts as an E3 ubiquitin ligase that targets c-Myb for nemo-like kinase (NLK)-induced degradation, J. Biol. Chem. 283 (2008) 30540–30548.
[41] C.H. Yeh, M. Bellon, J. Pancewicz-Wojtkiewicz, C. Nicot, Oncogenic mutations in the FBXW7 gene of adult T-cell leukemia patients, Proc. Natl. Acad. Sci. U. S. A. 113 (2016) 6731–6736.
[42] Y. Xu, T. Sengupta, L. Kukreja, A.C. Minella, MicroRNA-223 regulates cyclin E activity by modulating expression of F-box and WD-40 domain protein 7, J. Biol. Chem. 285 (2010) 34439–34446.
[43] M. Welcker, B.E. Clurman, Fbw7/hCDC4 dimerization regulates its substrate interactions, Cell Div. 2 (2007) 7.
[44] M. Welcker, E.A. Larimore, J. Swanger, M.T. Bengoechea-Alonso, J.E. Grim, J. Ericsson, N. Zheng, B.E. Clurman, Fbw7 dimerization determines the specificity and robustness of substrate degradation, Genes Dev. 27 (2013) 2531–2536.